Visible to Near-infrared Spectrum Reconstruction with Dielectric Metasurfaces

Kaikai Gao(高凯凯), Peiyang Li(李佩洋), Jiayi Wang(王佳怡), Sheng Liu(刘 圣), Peng Li(李 鹏), Dexing Yang(杨德兴), Jianlin Zhao(赵建林) and Dandan Wen(温丹丹)*

Key Laboratory of Light Field Manipulation and Information Acquisition, Ministry of Industry and Information Technology, and Shaanxi Key Laboratory of Optical Information Technology, School of Physical Science and Technology, Northwestern Polytechnical University, Xi'an 710129, China

*Corresponding author: dandanwen@nwpu.edu.cn

The miniaturization of spectrometers has received much attention in recent years. The rapid development of metasurface has provided a new avenue for creating more compact and lightweight spectrometers. However, most metasurface-based spectrometers operate in the visible light region, with much fewer research on near-infrared wavelengths. This is possibly caused by the lack of effective metasurface filters for the near-infrared light. This paper designs and fabricates a polarization-insensitive amorphous silicon metasurface, which exhibits unique transmission spectra in parts of the visible and near-infrared wavelengths. By passing the light to be measured through a metasurface filter array and measuring the transmitted power, we achieve precise reconstruction of unknown spectra in the visible and near-infrared range (450-950 nm) using an algorithm matched to the filter model. Our approach is a step towards miniaturized spectrometers within the visible- to near-infrared based on metasurface filter arrays.

Keywords: metasurfaces; filters; spectral reconstruction; algorithm

1. Introduction

Traditional spectrometers, primarily composed of wavelength-selective devices and detectors, are usually bulky and therefore limiting their applications in some scenarios. With the rapid development of metasurface technology in recent years[1], a new pathway has emerged for achieving more compact and lightweight spectrometers[2, 3]. Metasurfaces, composed of two-dimensional subwavelength structures, demonstrate diverse and flexible control over optical parameters such as amplitude, phase[4, 5], polarization[6-8], and spectrum[9], providing a novel platform for the design of miniaturized, high-performance micro-nano optical devices. Customizing the spectral control capabilities of metasurfaces allows them to serve as broadband filters with specific spectral response characteristics in computational spectrometers[10]. Compared with traditional narrowband filters, it is possible to use fewer metasurface filters to reconstruct spectra over a broader wavelength range.

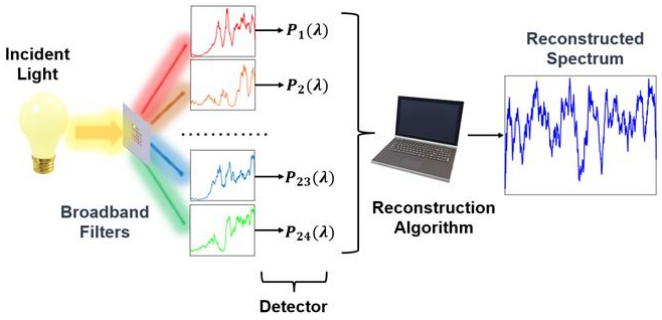

Fig. 1. Schematic of the silicon metasurface-based spectra reconstruction method. The incident spectral information is encoded by broadband filters, measured by a detector, and reconstructed using linear regression, aimed at minimizing the sum of squared differences between the measured results and the ground truth.

Recently, Xiong et al. demonstrated a silicon real-time ultraspectral imaging chip based on reconfigurable metasurfaces, comprising 155,216 (356 × 436) image-adaptive microspectrometers with ultra-high center-wavelength accuracy of 0.04 nm and spectral resolution of 0.8 nm[11]. Wang et al. adjusted the period, lattice constant, and hole sizes of photonic crystals, effectively controlling the transmission spectra in different regions. They coupled incident light from free space into lateral propagation modes, focusing it effectively at an imaging plane 1 mm from the metasurface array, achieving a 1 nm resolution spectrometer in the 550–750 nm range[12]. Yang et al., addressing the limitations of regular-shaped meta-atoms in traditional metasurfaces that restrict spectral imaging performance, proposed a new algorithm for generating freeform shaped meta-atoms with controllable feature sizes and boundary curvatures to enrich the spectral response of metasurfaces. They achieved a ultraspectral imager composed of a metasurface layer, microlens layer, and image sensor layer[13]. However, most miniature computational spectrometers based on metasurfaces mainly target the visible light range, with few devices capable of covering both visible and near-infrared wavelengths.

In this paper, we demonstrate visible to near-infrared spectrum reconstruction using metasurface filters consisting of amorphous silicon nanopillars. By varying period and size of the nanopillars, we can achieve rich transmission spectral features due to multimode resonances[14, 15]. These metasurface filterers enable effective control over parts of the visible and near-infrared spectra and with low correlation between different filters.

As shown in Fig. 1, the light to be measured illuminates the metasurface filter array, and the transmitted light power from each filter is measured by a photodetector. With the measured power and the known transmission spectra of the metasurface filters, we reconstruct the spectra of the incident light using an algorithm matched to the filter model[16, 17]. Both narrow and broadband spectra reconstruction (450 nm-950 nm) are achieved. The metasurface filter array used in this study is 2 mm × 2 mm in size and 0.7 mm in thickness, thus enabling integration with detectors such as CCDs and facilitating snapshot spectral measurement and sensing capabilities[18].

2. Results

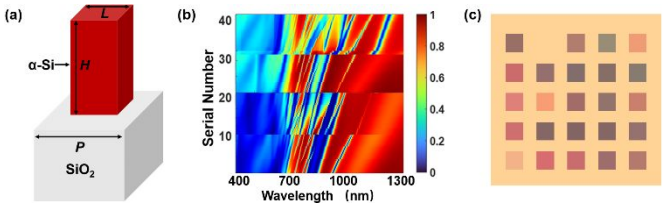

Fig. 2. Schematic and color filtering functions of metasurfaces. (a) Schematic of the metasurface unit structure. The substrate is glass, and the metasurface consists of square amorphous silicon pillars with a period of P, side length of L, and height H. (b) Simulation results of the transmission spectra for different metasurfaces. The horizontal axis represents the wavelength of the incident light, and the vertical axis represents serial number of the metasurfaces with different P and L values. The transmission is indicated by color; (c)Magnified optical images of a metasurface array with different L and P, where each metasurface, originally measuring 280 μm × 280 μm, forms an image magnified to approximately 1 cm × 1 cm.

As shown in Fig. 2(a), the metasurface consists of periodically arranged amorphous silicon nanopillars with a unit period, P, selectable among 350 nm, 400 nm, 450 nm, 500 nm, and 600 nm. The ratio of the pillar side length L to the period P ranges between 1/3 and 2/3, with a fixed height H of 620 nm. As the silicon pillars are square-shaped, they exhibit polarization-insensitive characteristics. Figure 2(b) presents the simulation results of the transmission spectra of different metasurfaces under normally incident broadband light. In the 400 nm to 700 nm range, the low transmission shown in blue are primarily due to the absorption of light in this spectrum by amorphous silicon. The changes in transmission beyond 700 nm is mainly caused by the excitation of dipole/multipole resonances in the nanostructures by incident light. When light near the bandgap frequency of the amorphous silicon illuminates the nanopillars, it not only excites electric dipole and magnetic dipole resonances but may also stimulate higher-order resonances such as electromagnetic quadrupole resonances[19, 20]. These resonances collectively enable control over the scattering properties of the nano-silicon structures, providing an effective way to design broadband filters for computational spectrometers[15]. In comparison, previous work has mostly focused on the filters in the visible light spectrum, and the geometrical parameters of the nanostructures are designed accordingly. For example, the silicon metasurfaces designed by Park et al.[21] have a maximum periodicity of no more than 400 nm. Their design has a height of 80 nm, and the diameters of the nanodisks are 80, 130, and 170 nm respectively. Although these designs perform well in filtering visible light, they do not consider filtering effects in the near-infrared region. In contrast, the silicon pillar metasurface we designed has a height of 620 nm, a maximum periodicity extending to 600 nm, and the side lengths of the nanopillars range from 150 nm to 400 nm, thereby providing effective filtering in the near-infrared spectrum as well.

Figure 2(c) shows the transmission images of the metasurfaces when illuminating by a white light source (Thorlabs tungsten halogen lamp SLS201L/M) and magnifying through an objective lens (Olympus PLN10X). The different colors in these images result from the specific transmission and absorption of light by different metasurface structures, as described in Fig. 2(b). The experiment results preliminarily prove the filtering functionality of our designed structure. Here we use 24 metasurfaces, each approximately 280 × 280 μm², collectively forming a transmissive broadband filter array.

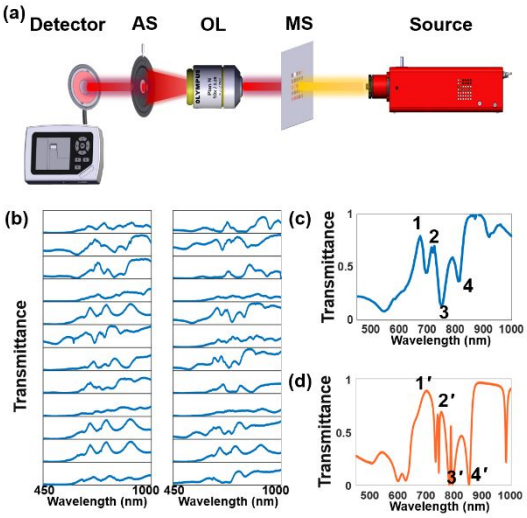

Fig. 3. Experimental setup and the transmission spectra. (a) Schematic of the experimental setup. MS: metasurface, OL: objective lens, AS: aperture stop. (b) Experimentally measured transmission spectra of the metasurface filter array. (c) Measured transmission spectra of a metasurface with P = 500 nm and L = 240 nm. (d) Simulation results of the transmission spectra for the same structure as in (c).

Figure 3(a) shows the experimental setup used to measure the transmission spectra of the metasurface filter array. The experiment employs a supercontinuum light source from a tunable filtering system, enabling precise measurement of transmission spectra in the 450 to 1000 nm wavelength range, with a step interval of 5 nm. The specific measurement process includes the following steps: First, the collimated beam from the laser illuminates the metasurface array, forming a magnified real image through the objective lens. The size of the real image is adjusted to be larger than the diameter of the small aperture of the aperture stop, ensuring that the measured part completely covers the small hole. The light beam then passes through the small hole and is received and measured by a power meter as the transmitted light power I_1. Subsequently, the metasurface is removed from the beam path, and the direct transmitted light power I_2 is measured. The transmission spectra at the corresponding wavelength are determined by calculating the ratio of I_1 to I_2. The measurement data is linearly interpolated with a precision of 1 nm, as shown in Fig. 3(b). Then, we compared the experiment results with the simulation results, as shown in Fig. 3(c)-(d). The positions of the four peaks and valleys, 1, 2, 3, and 4 in Fig. 3(c) correspond to the positions of 1', 2', 3', 4' in the simulation result in Fig. 3(d), respectively. Due to errors introduced in the manufacturing process, the experiment results exhibit a certain blue shift compared with the simulation results, but both are fundamentally consistent, demonstrating the accuracy of the simulation model and the effectiveness of the experimental setup. The reasons for the absence of high-frequency information are similar to those for the blue shift, and are due to errors in experimental fabrication. For example, the size and shape of nanopillars may be different from design.

In the following we describe the algorithm to reconstruct the spectrum of light under test. Assume $R_0(\lambda)$ represents the intrinsic response of the photodetector, which refers to the detector's sensitivity to light signals of different wavelengths, determined by the material and design of the detector. Let $T_k(\lambda)$ be the transmission

spectra of the k-th metasurface filter. Then, the overall response of the metasurface filter and the detector, $R_k(\lambda)$, can be expressed as

$$R_k(\lambda) = R_0(\lambda)T_k(\lambda),\ k = 1, 2, ..., N\#\quad (1)$$

Where, N is the number of metasurface filters. When the incident broadband light passes through the k-th metasurface filter, the total optical power is calculated as

$$P_k = \int_{\lambda_1}^{\lambda_2} [R_k(\lambda)P(\lambda) + n_k(\lambda)]d\lambda\#\quad (2)$$

Where, $P(\lambda)$ represents the power density of the light under test, $n_k(\lambda)$ is the system noise, and λ_1, λ_2 are the boundaries of the spectrum under test. Since $P(\lambda)$ is only unknown, it can be reconstructed from the measured power P_k of N photodetectors and the known detector response spectra $R_k(\lambda)$.

In practical applications, the elements of Equation (2) are discretized and expressed in vector form. Specifically, $R_k(\lambda)P(\lambda)$ is discretized into $\boldsymbol{R_k}[\lambda]$ and $\boldsymbol{P}[\lambda]$. This approach involves representing the spectral response of the k-th filter and the power density of the light as matrices. $\boldsymbol{R_k}[\lambda]$ is configured as an M-row, 1-column matrix, where each row corresponds to the response coefficient at a specific wavelength λ, and $\boldsymbol{P}[\lambda]$ is also an M-row, 1-column matrix, each row representing the intensity of the incident light at a specific wavelength λ. This matrix representation allows for the systematic computation and analysis of spectral data.

When multiplying $\boldsymbol{R_k}[\lambda]$ by $\boldsymbol{P}[\lambda]$, we obtain a linear equation, and with N detectors, we have a system of N linear equations. Theoretically, this system should have a unique solution when $N = M$, allowing us to solve for the unknown spectral data from the known response matrix and measured values. However, in practice, the number of detectors N is often less than the number of reconstruction points M, and due to measurement errors and noise, these linear equations may become inconsistent, i.e., without an exact solution. This noise could originate from instrument errors, environmental interference, or inaccuracies in data processing. Despite these challenges, we can still approximate a solution to these equations using the least squares method to find a set of spectral data that minimizes the error between them and the measured data[3].

To validate the quality of spectral reconstruction, we employed a supercontinuum light source and a tunable filtering system to produce narrowband spectra. This was achieved by adjusting the supercontinuum laser to emit a set of beams around the target wavelength. For instance, the narrow band at 850 nm consists of a beam at 850 nm, complemented by beams at 852 nm and 848 nm with lower power. This is due to the inherent characteristics of the supercontinuum laser. We found that the spectrum of the low-power 850 nm output, measured by a commercial spectrometer, was unstable and oscillating. However, when low-power output at 848 nm and 852 nm were also introduced, the measured spectrum became stable and is conductive to the reconstruction. A commercial spectrometer (Thorlabs, CC200/M, measurement range: 200 nm-1000 nm) was used to measure these narrowband spectra as shown by the blue solid lines in Fig. 4(a)-(f), allowing for comparison with the reconstructed spectra. In this study, we implemented spectral reconstruction using the non-negative linear least squares algorithm, which finds a set of solutions that minimize the sum of squared differences between predicted and actual values while ensuring that the solution vector remains non-negative. This method is suitable for spectral data reconstruction, as spectral intensities cannot be negative. The mean squared error (MSE) was employed to assess the quality of the reconstructed spectra. The results show that the peak wavelengths of each reconstructed spectrum closely match the corresponding reference spectra, with the MSE for narrowband reconstructed spectra at 500 nm, 600 nm, 700 nm, 760 nm, 850 nm, and 950 nm ranging between 0.0017 and 0.0040. For narrowband spectra reconstruction, it is capable of effectively distinguishing light

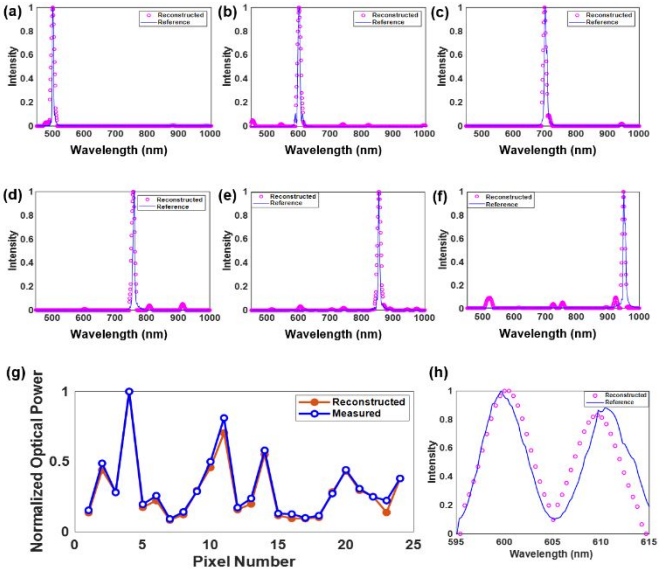

Fig. 4. Experimentally reconstructed spectra of narrowband light sources and comparison of measured and reconstructed power. (a)-(f) Reconstructed spectra of narrowband light sources at different wavelengths compared with spectra measured by a spectrometer. The central wavelengths and full width at half maximum (FWHM) are: 500 nm (FWHM: 4.32 nm), 600 nm (FWHM: 4.71 nm), 700 nm (FWHM: 9.48 nm), 750 nm (FWHM: 6.49 nm), 850 nm (FWHM: 5.50 nm), 950 nm (FWHM: 9.83 nm). (g) Comparison of measured and reconstructed normalized light power with narrowband light sources centered at 600 nm. (h) Reconstruction results of the double peaks corresponding to the 600 nm and 610 nm spectral lines.

at intervals of 10 nm. While the shapes of the reconstructed spectrum peaks generally align with the reference spectra, there are differences, such as in reproducing fine features and peaks at low intensities, possibly due to the limited number of filters used. Increasing the number of filters could further improve the quality of the reconstructed spectra. In Fig. 4(g), we demonstrate the comparison between the measured transmitted light power (blue curve) and the calculated light power (red curve) when illuminating 24 metasurface filters with a narrowband light source centered at 600 nm [same as the one used in Fig. 4(b)]. The reconstructed spectra with the previously measured overall response of the metasurface filter/detector are used to estimate the light power value. Comparing the measured light power with the estimated light power allows for assessing the accuracy of the spectral reconstruction. This approach offers the advantage of providing a direct and intuitive verification of the spectral reconstruction effectiveness and allows for a quantitative analysis of errors in the reconstruction process, such as those caused by environmental noise. It is evident that the measured light power and the light power calculated using the reconstructed spectrum generally match well. The discrepancies between some filter results and the measured outcomes can be attributed to inaccuracies in the measurement of intrinsic responsivity and the influence of environmental noise[22].

For the reconstruction of broadband spectra, we employed the Least Absolute Shrinkage and Selection Operator (Lasso) regression algorithm combined with a Gaussian filter to enhance accuracy. This

approach helps avoid overly complex models that fit too closely to specific data (a problem known as overfitting), thereby improving the model's performance on new, unseen data. This characteristic makes Lasso particularly useful for spectrum reconstruction, as it ensures that only the most relevant features are considered, making the model both simpler and more effective. Gaussian filtering helps data smoothing through weighted averaging. In the context of spectra reconstruction, the Gaussian filter is utilized to smooth the data, removing noise and improving signal quality. In this study, the specific parameters of the Gaussian filter (standard deviation 1.8, window size 150) were determined through training to ensure the best fit for our model. The standard deviation parameter controls the degree of smoothing, with a larger value implying stronger smoothing and a smaller value retaining more detail. The window size dictates the number of data points considered for averaging, with larger windows encompassing more points and thus yielding smoother results. The choice of these parameters depends on the specific spectral characteristics and desired reconstruction accuracy in practical applications. Adjusting and optimizing these parameters can effectively improve the accuracy and reliability of spectral reconstruction. As shown in Fig. 5(a)-(b), the two original spectra for reconstruction are obtained from an LED light source (wavelength range: 500 nm-700 nm) through green (bandwidth 485 nm-565 nm) and red filters (bandwidth 600 nm-2500 nm), respectively. The spectrum in Fig. 5(c) is produced using a tungsten halogen lamp source (bandwidth: 360 nm-2400 nm) after passing through a cutoff filter (bandwidth 485 nm-1100 nm) and a broadband filter (650 nm-2500 nm). It is evident that the reconstruction of broadband spectra also matches the measurements from the commercial spectrometer.

Improvements in spectral resolution and reconstruction accuracy

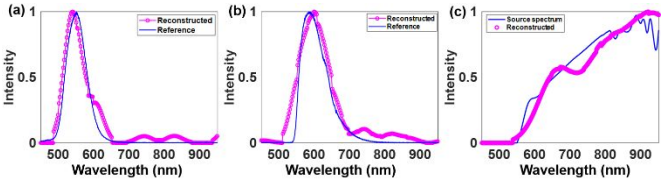

Fig. 5. Reconstructed spectra of broadband light sources. (a) Reconstructed result of a white LED light through a green filter (bandwidth 485 nm - 565 nm) and (b) through a red filter (bandwidth 600 nm-2500 nm). (c) Reconstructed result of a Thorlabs tungsten halogen lamp SLS201L/M through a cutoff filter (bandwidth 485 nm-1000 nm) and a broadband filter (650 nm-2500 nm).

can be achieved by reducing measurement errors. This includes using more stable calibration light sources and employing higher-performance transmittance detection equipment. Additionally, increasing the number of broadband filters helps enhance spectral resolution, as these filters can cover a wider spectral range, enabling a broader spectrum reconstruction. On the other hand, enhancing spectral resolution and reconstruction accuracy also relies on utilizing prior spectral knowledge (such as signal sparsity) and advanced reconstruction algorithms. Methods like L1 and L2 regularization norms, Principal Component Regression (PCR), and genetic algorithms can effectively improve spectral reconstruction accuracy. These algorithms, by considering specific features and structures of spectral data, can more accurately recover and reconstruct spectral signals. By integrating these techniques, the accuracy and reliability of spectral analysis can be significantly enhanced.

3. Conclusion

In this paper, we proposed and experimentally validated a spectral measurement method based on metasurface filters. These filters, composed of amorphous silicon-based nanopillars, have a responsive range covering visible to part of the near-infrared spectrum (450 nm-950 nm) and exhibit rich spectral characteristics. After passing through the filter, the spectral information of the light under test can be reconstructed based on its intensity information. The experiment successfully achieved precise reconstruction of both narrowband and broadband unknown spectra in parts of the visible and near-infrared wavelengths. Therefore, this method has broad application prospects in fields such as chemical analysis, biomedical research, and environmental monitoring.

Fabrication Process

The process involved depositing a 620 nm thick amorphous silicon (a-Si) thin film on a 700 μm thick glass substrate using Plasma Enhanced Chemical Vapor Deposition (PECVD). A 100 nm thick layer of hydrogen silsesquioxane electron beam lithography resist (HSQ, XR-1541) was then spin-coated onto the film and baked on a hot plate at 100 °C for 2 minutes. Subsequent patterning of the resist was carried out using standard electron beam lithography (EBL, Nanobeam Limited, NB5), followed by development in an NMD-3 solution (2.38% concentration) for 2 minutes. Finally, the designed patterns were transferred from the photoresist to the amorphous silicon film using Inductively Coupled Plasma Etching (ICP, Oxford Instruments, Oxford Plasma Pro 100 Cobra300, SF6:C4F8 = 19.8sccm: 40.2sccm).

Acknowledgements

This work was supported in part by the National Natural Science Foundation of China (Grant No. 62175200) and the National Key Research and Development Program of China (2022YFA1404800).

Conflict of interest

The authors declare no conflict of interest.

References

1. Q. Yuan, Q. Ge, L. Chen et al., "Recent advanced applications of metasurfaces in multi-dimensions," Nanophotonics **12**, 2295-2315 (2023).
2. Z. Yang, T. Albrow-Owen, W. Cai et al., "Miniaturization of optical spectrometers," Science **371**, eabe0722 (2021).
3. L. Gao, Y. Qu, L. Wang et al., "Computational spectrometers enabled by nanophotonics and deep learning," Nanophotonics **11**, 2507-2529 (2022).
4. J. Li, Y. Yuan, Q. Wu et al., "Dual-band independent phase control based on high efficiency metasurface [Invited]," Chin. Opt. Lett. **19**, 100501 (2021).
5. H. Wang, Z. Zhang, K. Zhao et al., "Independent phase manipulation of co- and cross-polarizations with all-dielectric metasurface," Chin. Opt. Lett. **19**, 053601 (2021).
6. D. Wen, F. Yue, G. Li et al., "Helicity multiplexed broadband metasurface holograms," Nat. Commun. **6**, 8241 (2015).
7. D. Wen, K. Pan, J. Meng et al., "Broadband Multichannel Cylindrical Vector Beam Generation by a Single Metasurface," Laser Photonics Rev. **16**, 2200206 (2022).
8. K. Pan, X. Wu, L. Zhou et al., "Vectorial holography for independent intensity and polarization control," Opt. Lett. **48**, 4217-4220 (2023).
9. W. Yang, S. Xiao, Q. Song et al., "All-dielectric metasurface for high-performance structural color," Nat. Commun. **11**, 1864 (2020).
10. W. Zhang, H. Song, X. He et al., "Deeply learned broadband encoding stochastic hyperspectral imaging," Light Sci. Appl. **10**, 108 (2021).
11. J. Xiong, X. Cai, K. Cui et al., "Dynamic brain spectrum acquired by a

real-time ultraspectral imaging chip with reconfigurable metasurfaces," Optica **9**, 461-468 (2022).
12. Z. Wang, S. Yi, A. Chen et al., "Single-shot on-chip spectral sensors based on photonic crystal slabs," Nat. Commun. **10**, 1020 (2019).
13. J. Yang, K. Cui, X. Cai et al., "Ultraspectral Imaging Based on Metasurfaces with Freeform Shaped Meta-Atoms," Laser Photonics Rev. **16**, 2100663 (2022).
14. S. Jahani, and Z. Jacob, "All-dielectric metamaterials," Nat. Nanotechnol. **11**, 23-36 (2016).
15. A. I. Kuznetsov, A. E. Miroshnichenko, M. L. Brongersma et al., "Optically resonant dielectric nanostructures," Science **354**, aag2472 (2016).
16. J. Bao, and M. G. Bawendi, "A colloidal quantum dot spectrometer," Nature **523**, 67-70 (2015).
17. S. Zhang, Y. Dong, H. Fu et al., "A Spectral Reconstruction Algorithm of Miniature Spectrometer Based on Sparse Optimization and Dictionary Learning," Sensors **18**, 644 (2018).
18. J. Lee, Y. Park, H. Kim et al., "Compact meta-spectral image sensor for mobile applications," Nanophotonics **11**, 2563-2569 (2022).
19. J. Proust, F. Bedu, B. Gallas et al., "All-Dielectric Colored Metasurfaces with Silicon Mie Resonators," ACS Nano **10**, 7761-7767 (2016).
20. A. Krasnok, M. Caldarola, N. Bonod et al., "Spectroscopy and Biosensing with Optically Resonant Dielectric Nanostructures," Adv. Opt. Mater. **6**, 1701094 (2018).
21. C. S. Park, V. R. Shrestha, W. Yue et al., "Structural Color Filters Enabled by a Dielectric Metasurface Incorporating Hydrogenated Amorphous Silicon Nanodisks," Sci. Rep. **7**, 2556 (2017).
22. J. Meng, J. J. Cadusch, and K. B. Crozier, "Detector-Only Spectrometer Based on Structurally Colored Silicon Nanowires and a Reconstruction Algorithm," Nano Lett. **20**, 320-328 (2020).